Oxygen Isotope Effect in High Temperature Superconductors

Samantha Rubeck

A thesis submitted to the

Honors Council of the University of Colorado-Boulder

in partial fulfillment of the requirements for the degree of

Bachelor of Arts

Department of Physics

March 30, 2015

This thesis entitled: Oxygen Isotope Effect in High Temperature Superconductors

written by Samantha Rubeck

has been approved for Departmental Honors in Physics

Daniel Dessau, Thesis Adviser | Physics

James Thompson, Honors Council Representative | Physics

Randal O'Reilly | Psychology and Neuroscience

Date

The final copy of this thesis has been examined by the signatories, and we find that both the content and the form meet acceptable presentation standards of scholarly work in the above mentioned discipline.

Oxygen Isotope Effect in High Temperature Superconductors

Samantha Rubeck

Abstract

Conventional superconductivity is described by its interactions of electrons through a specific vibrational mode called phonons. For high temperature superconductors (HTS), the mechanism which explains its superconductivity is still unknown. Various measurement techniques have been established to study the mechanism behind HTS including looking at the effect of altering the mass of oxygen in the copper-oxide planes of cuprate crystal lattices from 16 g/mol to 18 g/mol, also known as the isotope effect. While the results of previous experiments are still inconclusive, I aim to investigate this effect using magnetometry, Raman spectroscopy, and laser angle resolved photoemission spectroscopy (ARPES) in order to find evidence for a particular pairing mechanism.

Acknowledgements

First off, I want to thank my adviser, Dan Dessau, for giving me the opportunity to work on this project. Without the hours and hours of guidance you have given me over the years, both in terms of this project as well as for graduate school, I would not have made it to where I am now.

I also want to thank all the members of the Dessau Group who have helped me over the years especially Steve Parham, Justin Waugh, Tom Nummy, and Justin Griffith who have gone above and beyond to help me. Thanks for your patience and ability to explain the same concepts multiple times.

Finally I would like to thank Jhih-An Yang for assisting me with the Raman spectroscopy measurements, my parents for all the emotional support, and the Undergraduate Research Opportunity Program for the financial support.

Contents

Chapter 1

Introduction

Superconductivity is a branch of condensed matter physics that was first discovered by Heike Kamerlingh Onnes in 1911 [Onn11]. Since then, many types of superconductors have been studied yet there are many aspects of superconductor properties that are not well understood. One area where this is prominent is in a class of materials called high-temperature superconductors (HTS). These quantum materials have been studied extensively both experimentally and theoretically but experts in the field have yet to reach a consensus on the underlying physics of the exotic phenomenon [Dou08].

In recent years, there have been many technological advances that have the ability to make a large impact in understanding HTS. One such advancement is low energy, laser angle-resolved photoemission spectroscopy (ARPES). This technique is used to explain the interaction between the electrons and the atoms in a solid. In this specific experiment, laser-ARPES, along with Raman spectroscopy and magnetometry, will measure the effect of oxygen isotope substitution (O16 to O18) in cuprate materials.

1.1 Conventional Superconductors

There are two main properties that define a superconductor: perfect conductivity and perfect diamagnetism [Sjö01]. Perfect conductivity is the feature that led

Kamerlingh Onnes to note that some materials transition to a superconducting state at a certain critical temperature. This enables electrons in a material to flow with zero resistivity (Figure 1.1). Therefore these materials do not produce losses of energy [Onn11].

Perfect diamagnetism, discovered by Meissner and Ochsenfeld in 1933 [MO33], is the property where there is complete magnetic expulsion in the material. In other words, B = 0 in the bulk of the material. If a magnetic field is applied to a material below the critical temperature value where the sample becomes superconducting, T_c, screening currents on the surface of the material are induced in order to expel all magnetic flux from the interior. If a magnetic field is applied above T_c, then the magnetic field is expelled from the interior of the material as it is cooled through T_c [Sjö01]. The screening currents that arise flow to produce a magnetic field that is equal in magnitude and opposite in direction to the applied field allowing the fields to cancel. Therefore it is the rise of these screening currents that expel the magnetic field from the interior (Figure 1.1). This is known as the Meissner Effect.

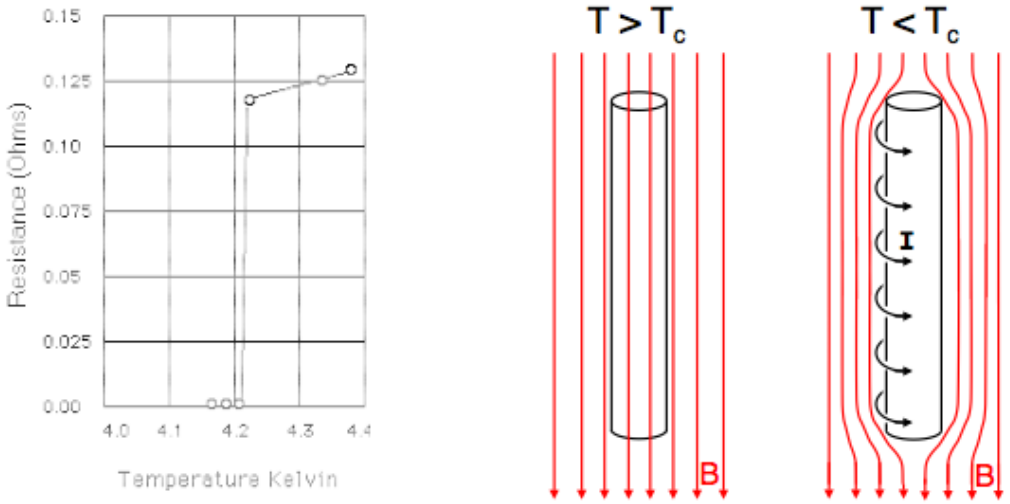

(a) Vanishing resistance (b) Meissner effect

Figure 1.1: a) This is data that experimentally proves perfect conductivity. As the material transitions into the superconducting state (by being cooled) the resistance in the material drops to zero. b) This image represents perfect diamagnetism in the superconducting state ($T<T_c$) due to currents produced on the surface of the material. [Hof03]

1.1.1 BCS Theory

So what is the underlying mechanism that causes superconductors to exhibit such unique and mysterious properties? In 1957, John Bardeen, Leon Cooper, and John Robert Schrieffer developed what is now known as the BCS theory of superconductivity, which eventually won them the Nobel Prize in 1972 [BCS57]. This theory succeeded in explaining many material properties of superconductors such as the band gap, heat capacity, and T_c. The building block of this theory relies on electron-electron interactions which form quasiparticles that are known as cooper pairs [BCS57].

Electrons, a spin-$\frac{1}{2}$ particle (fermion), in a solid determine the main properties of a material. In conductors, once the valence electrons of the lattice structure have enough energy to get out of the ground state (i.e. they have more energy than the band gap), a "sea of electrons" forms. The resistance associated with conductors forms due to these electrons scattering off of the lattice structure, impurities, and other features of the material. When two electrons pair up though, as they do for superconductivity, the resulting system acts like an integer spin particle (boson). Since bosons do not obey the Pauli Exclusion Principle, it is energetically favorable for electrons to be in the same quantum mechanical ground state [Roh94] This means that these Cooper pairs are condensates that have the same wave function and can move through a lattice with the same momentum without scattering (zero electrical resistance).

Cooper pairing, as explained by BCS theory, forms due to vibrational modes in the lattice structure (one might think of masses on springs where the masses are the atoms and the springs are the bonds between atoms). These modes of vibration are called phonons. Phonons are a type of vibration that mediate sound waves in solids. The phonons cause regions of the lattice structure to be more positive than other regions. This provides an attractive force that is stronger than the Coulomb repulsion of near-by electrons resulting in these electrons, which have equal but opposite momentum, to pair (Figure 1.2) [Frö50]. Once again, it is energetically

favorable to allow these electrons to pair since the energy required to scatter the paired electrons (determined by the size of the superconducting gap) is very large at the Fermi surface (described in more detail later in the chapter) [Hof03].

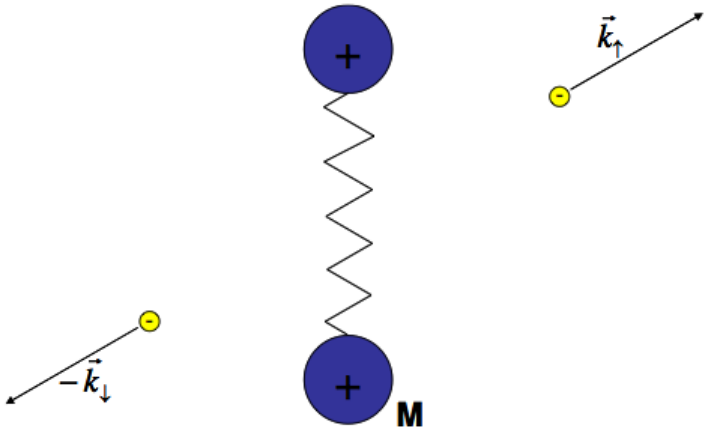

Figure 1.2: A phonon brings two positive ions closer together and makes that region of space more positive than surrounding regions. This attracts electrons of opposite spin and momentum to occupy the same space (i.e. paring). [Dou08]

The two of the most important outcomes of BCS theory are its prediction of the energy gap and its ability to explain the experimentally seen isotope effect (see subsection "Isotope Effect") [Hof03]. In solids, each material has an associated energy gap that needs to be overcome for the electron to not be bound. By understanding these microscopic electronic properties, macroscopic features can then be explained.

In BCS theory, the superconductor's band gap (at zero temperature) is predicted to be

$$\Delta(T \to 0) \approx 1.75\, k_B T_c \tag{1.1}$$

where k_B is Boltzmann's constant.

At temperatures approaching T_c the size of the gap is predicted to be

$$\Delta(T \to T_c) \approx 3.2\, k_B T_c \sqrt{1 - (T/T_c)} \tag{1.2}$$

These equations show that the superconducting gap, which depicts how electrons

are bound to the lattice, approaches zero near T_c and a maximum value at T=0 K. This is important because it shows that above the superconducting transition temperature, there is no gap and therefore the properties of electrons in the material before it super-conducts is distinct from the electron properties below T_c [BCS57].

The dependence of the superconducting gap as a function of temperature given by Equation 1.1 and Equation 1.2 was also experimentally proven by Sutton and Townsend (seen in Figure 1.3). At the critical temperature, there is no superconducting gap and as T approaches zero, the normalized gap amplitude approaches its maximum value. This is important because it shows that there is a universal temperature dependence on the size of the gap, regardless of the material [Bla92].

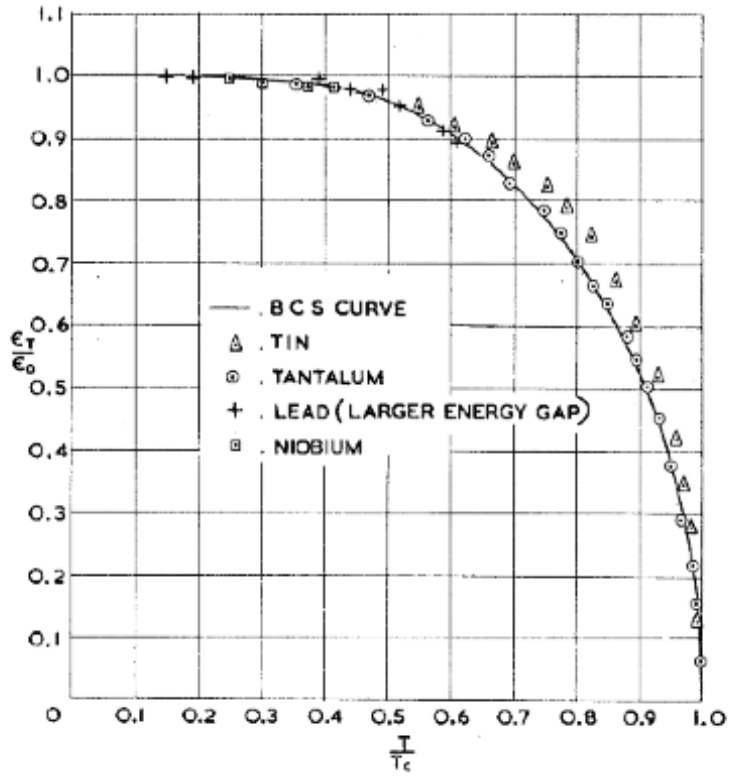

Figure 1.3: Experimental data of the superconducting gap for a variety of material and BCS predictions. This shows the existence of a universal temperature dependence on gap size. [TS62]

The BCS theory also reproduces the isotope effect, which is the experimental technique used to relate critical temperature and mass. Specifically, the critical temperature is inversely proportional to the mass of the isotope used in the material [Rey+50].

The choice of isotope affects the frequency of lattice vibrations. This effect suggests that superconductivity is related to vibrations of the lattice, which is incorporated in BCS theory (where lattice vibrations act as the binding mechanism of electrons in a Cooper pair).

1.1.2 Isotope Effect

The fact that a change in isotope affects the frequency of lattice vibrations can be explained using Einstein's model of solids on a spring [Sim13]. In this model atoms are treated like masses on springs, each of which has a frequency of

$$\omega_0 = \sqrt{\frac{k}{m}} \tag{1.3}$$

Therefore by changing the mass of the system, the frequency of lattice vibrations also change.

The macroscopic property, T_c, also has a dependence on the masses in the lattice which implies that phonon vibrations offer a good explanation of underlying superconducting properties. For example, by substituting mercury-202 with mercury-198, the T_c increased proving the dependence of superconductivity on lattice vibrations (reference Figure 1.4) [Max50].

This relation can be written as:

$$T_c \propto M^{-\alpha} \tag{1.4}$$

In conventional superconductors, the alpha factor in Equation 1.4 is experimentally measured and theoretically predicted (by BCS theory) to be approximately 0.5. In HTS, the alpha factor varies greatly and is dependent on the doping of the material and its temperature [Ami11].

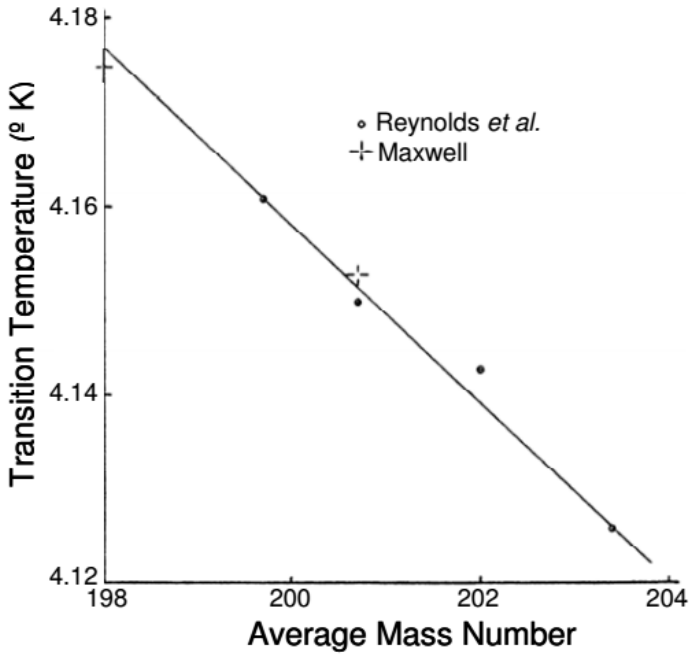

Figure 1.4: Experimental data of the isotope effect using various isotopes of mercury. [Dou08]

1.2 High Temperature Superconductors

When Georg Bednorz and Alex Müller first discovered high temperature superconductivity (materials having a T_c above 30K) in 1986 [BM86], the seemingly understood phenomenon produced a plethora of new research. Since BCS theory predicted a critical temperature upper limit of 30K, these higher temperature materials could not be explained by this widely accepted theory [BCS57]. Experts in the field needed a new way to explain this groundbreaking phenomenon. The most obvious step is to look for phonons using the isotope effect. Thus far though, isotope effect experiments have been inconclusive. Research using angle resolved photoemission spectroscopy (ARPES) [Gwe+04], SQUID and torque magnetometry and X-ray absorption near edge spectroscopy (XANES) [Zha+97][ZKC01], and other techniques point towards a phonon mode interaction in the electronic structure of HTS. Other experimental and theoretical [Sca99][USG04] techniques such as inelastic neutron scattering [CSB99][USG04] and infrared spectroscopy [CSB99] looked at the transport and nuclear resonances and found that they coincide with spin fluctuations associated with magnetic excitations [Dai+99]. There was even an

experiment done using infrared spectra which concluded that the pairing mechanism is neither magnetic resonance nor phonons [HTG04].

One of the reasons that this has been so difficult to study is due to the fact that there is not a symmetric pairing potential across the Fermi surface of these materials (described in more detail in the following section). In conventional superconductivity the pairing potential is symmetric (s-wave gap). In HTS the pairing potential is not symmetric so electrons traveling along one direction in the crystal feel a different pairing potential than electrons traveling in another direction (d-wave gap) [Hof03].

Another issue in understanding these materials is that everything in the system is highly correlated [She+02]. Changing one aspect of the material (like doping or removing an electron) changes how all the other electrons interact in the system. This creates a situation where probing properties of HTS in itself changes the system instead of just studying the system.

1.2.1 Cuprate Structure

One of the most common materials to study in isotope experiments is $Bi_2Sr_2CaCu_2O_{8+x}$ (BSCCO). These materials, also known as cuprates, contain copper oxide layers that play a pertinent role in this quantum phenomenon. More specifically, they are the layers where superconductivity occurs. In other words, cooper pairs and the Meissner current loops both form on these layers. The greater the number of copper oxide layers in a material, the larger the value of T_c [Che+07] The samples used in this isotope experiment are optimally doped BSCCO-2212 with two copper oxide (Cu-O layers (see Figure 1.5). It is the oxygen in these layers that get substituted from a mass of 16 g/mole to a mass of 18 g/mole. This is important because if there is a shift in electronic properties due to the mass substitution, then we can attribute it to phonons in the Cu-O layers, where the mass was substituted.

A universal property of HTS is its Fermi surface (Figure 1.5). The Fermi surface is a cut of the momentum space at the Fermi energy [Sim13] which is the energy point that separates unfilled orbitals and filled orbitals at zero kelvin [Sim13]. The

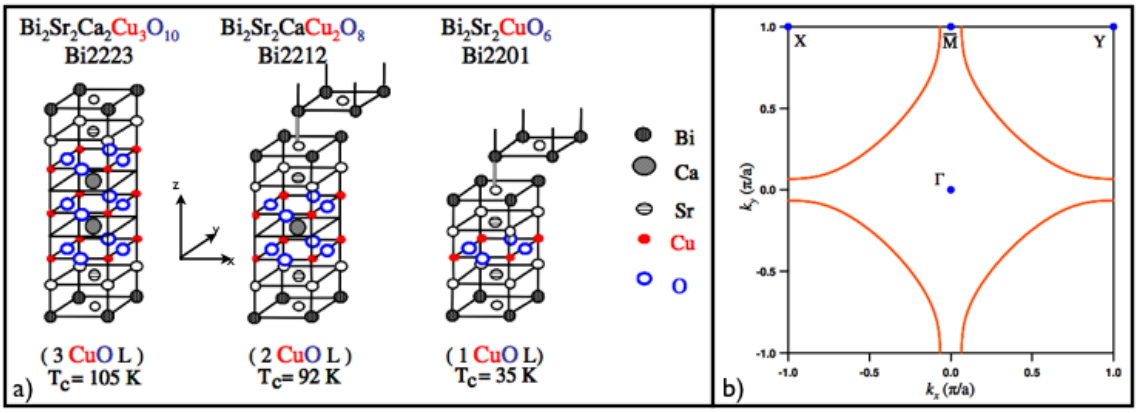

Figure 1.5: a) These are the basic lattice structures of BSCCO. This shows the dependence of critical temperature on the number of Cu-O layers. In this experiment we are using Bi2212 (the middle structure). b) This is the 2D Fermi surface of BSCCO. [Dou08]

important thing to note about BSCCO Fermi surface is its high symmetry directions [Dou08] which have relations to the superconducting gap. This includes the nodal direction (ΓY) and the antinodal direction (ΓM). It was shown that along the node, the superconducting gap goes to zero and along the antinode it goes to a maximum value [She+93]. Note that this Fermi surface is only a 2D cut rather than a full 3D surface. This is due to the fact that we can treat BSCCO as a quasi-2D structure since the conduction occurs only in the Cu-O planes. Therefore the z-axis momentum in the Fermi surface is not needed.

Chapter 2

Experimental Design

In order to understand the electronic mechanisms in HTS, we must first characterize each sample and then proceed to probe its electronic properties. The experimental approach to this is threefold: magnetometry (determines critical temperature), Raman spectroscopy (verifies isotope substitution on phonon modes), and laser angle resolved photoemission spectroscopy(maps out momentum and energy space to study electronic interactions in the lattice). This section will focus on these three techniques as well as the advantages that they offer for studying the isotope shift.

2.1 Magnetometry

Magnetometry, first invented by Carl Friedrich Gauss in 1833 [Mal07], is a method used to map out magnetic field lines both in terms of strength and direction. In the Dessau Group magnetometry is used to study the critical temperature, T_c, of HTS. The magnetometer used in this experiment, which is a home-made device, employs the method of mutual inductance. The physical setup of this device uses two coils, each on opposite sides of the sample parallel to the sample's x-y plane (see Figure 1.5). On one side is the driver coil, which has an AC current. This AC current produces an AC magnetic field. The other coil is the pick-up coil. This coil generates a current due to this AC magnetic field. When the sample that is wedged between these two coils is in the normal state, the magnetic field penetrates

the sample. In other words there is magnetic flux through the superconductor. The pick-up coil detects this magnetic coil and produces an output current. When the sample is in the superconducting state the Meissner effect takes over and expels the magnetic field generated by the driver coil from the sample. This shielding prevents the AC field from reaching the pick-up coil and in turn prevents the pick-up coil from producing a current. In theory, if the sample was infinitely long, the pick-up coil signal would drop to zero. Due to the fact that these samples are of finite size and that often the sample is smaller then the radius of the coils, some of the signal still gets detected by the pick-up coil. Therefore when T_c is reached we see a drop in signal and the size of this drop is proportional to the size of the sample. Note that this magnetometer only measures the magnitude of the magnetic field as derived from the pick-up current and not the direction of the field.

There are several advantages to using the method of mutual inductance as opposed to other techniques such as resistivity measurements. Most importantly, it does not damage the sample because there is no direct electrical contact. Another advantage is that it examines the sample more uniformly than other methods. This is because the super-currents that create the Meissner effect must flow around a large outer layer in order for the drop in signal to be observed [Mye93].

Figure 2.1 shows the layout of the magnetometer. Within the removable insulating square piece lies one of the coils while the other lies in an insulating square at the base of rod. The sample gets placed in-between this removable square and the rod. Next to the coils lies the heater and the diode. The heater is used to vary the temperature of the sample at different speeds from both low to high and high to low temperatures. The diode measures the temperature on the copper base of the magnetometer. The diode used is a semiconductor junction that measures temperature by detecting a change in voltage along the forward direction of the diode. One advantage to using diodes to measure temperature is that they have a nearly linear relationship between temperature and voltage applied [GK12]. Originally, it was assumed that the temperature at the diode is equivalent to the temperature of

the sample (which is located 15mm below the diode). This is incorrect and implies that the diode is not always measuring an accurate T_c value.

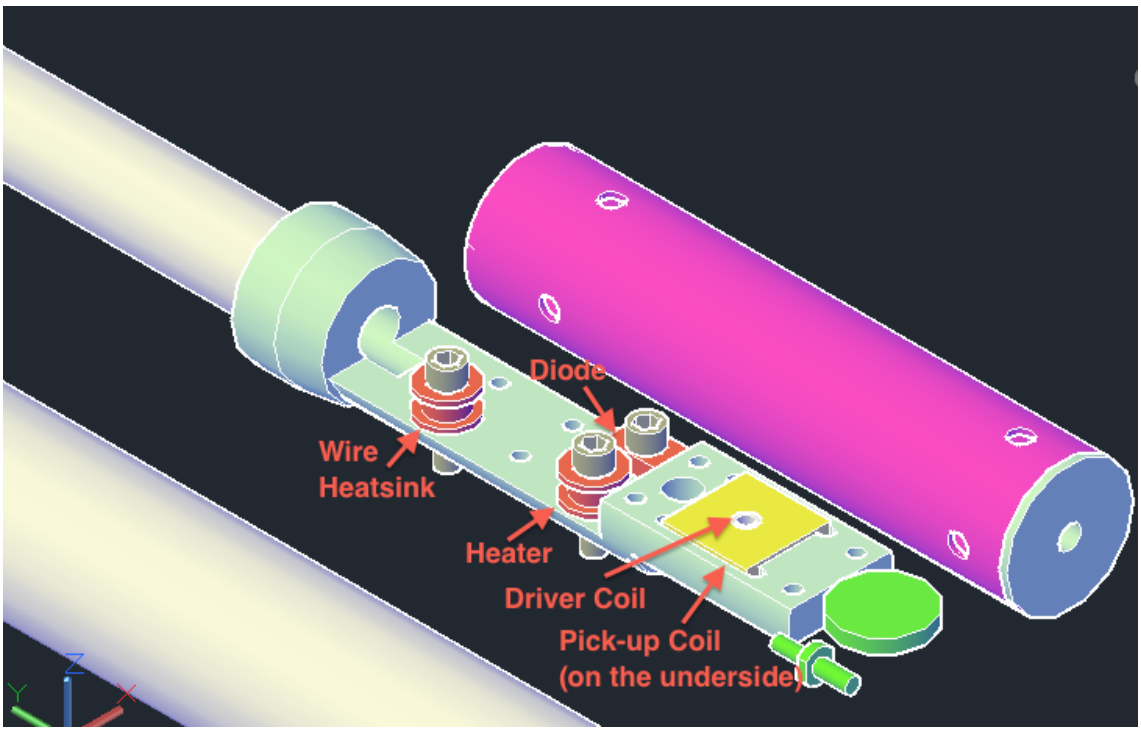

Figure 2.1: Figure made by Justin Griffith. The position of the driver coil and pick-up coil are not necessarily in this order. The rod that holds the these elements is made out of copper (used for its high thermal conductivity at cold temperatures).

Figure 2.2 shows a zoomed in view of the coil/sample setup. Note that the x-y plane of the sample and the magnetic field are perpendicular to each other. This allows for the maximum value of Meissner currents to form in the copper oxide planes.

Before the sample is placed in the magnetometer, it is first put in a magnetometer packet. The magnetometer packet is composed of lens tissue that is folded into a pocket which is then sealed by tape. This packet acts as protection from dirt and other surface damages that might otherwise occur.

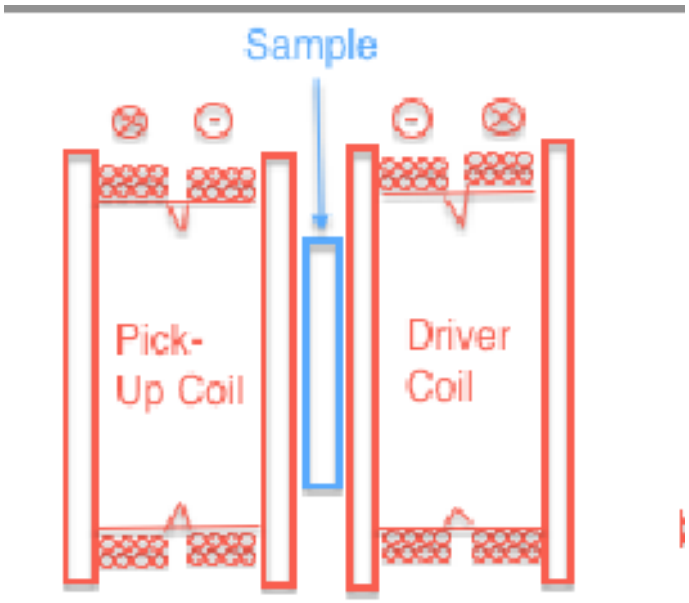

Figure 2.2: This image shows the sample placement in terms of the driver and pickup coil.

2.1.1 Uncertainties in Magnetometry

Hysteresis

There are two ways of defining hysteresis. One is that there is a dependence of a system on its past. This is considered a type of "memory" where if the input alternately increases and decreases, the output produces a hysteresis loop. This is an intrinsic explanation of hysteresis and is exemplified in the magnetic relaxation of vorticies (when HTS are above a critical magnetic field H_c). This would also cause energy dissipation and in turn, a hysteresis effect [Sjö01]. This critical field value is several orders of magnitude larger than the magnetic field produced by the magnetometer therefore vorticies are not the source of hysteresis in this experiment.

An alternate way to define hysteresis is extrinsically. This kind of hysteresis represents a lag between the input and the output due to its environment. The magnetometry measurements in this experiment exhibit this type of hysteresis. In our case, the hysteresis is due to a gradient of thermal conductivity (a material's ability to conduct heat) between the sample and the diode.

The hysteresis in this setup is due to thermal effects. Since the sample is in

a thermally isolated packet, the thermal syncing between the sample and diode has decreased. So as the sample becomes superconducting, there is a difference in the actual temperature that the sample is experiencing and the temperature that the diode is reading. When the sample is being ramped down, the diode reads a temperature that is colder than the actual T_c value. When the sample is being ramped up, the diode reads a temperature that is warmer than the actual T_c value. We see that the sample lags behind the heater/diode because the heater and diode are thermally connected (on the same copper rod) as compared to their connection to the sample. In other words, this lag occurs because the sample is not thermally sunk to the copper rod.

The faster the ramping done by the heater, the larger the hysteresis effect. Since the hysteresis is set by the thermal conductivity of the copper rod, when you ramp the system faster, a larger thermal gradient gets built up between the copper and the thermally isolated sample. This in turn creates a large hysteresis effect. As the ramping slows down, the thermal gradient gets smaller and the hysteresis decreases. The relationship between ramping speed and hysteresis size is shown in Figure 2.3, which uses a linear fit for lack of a better model.

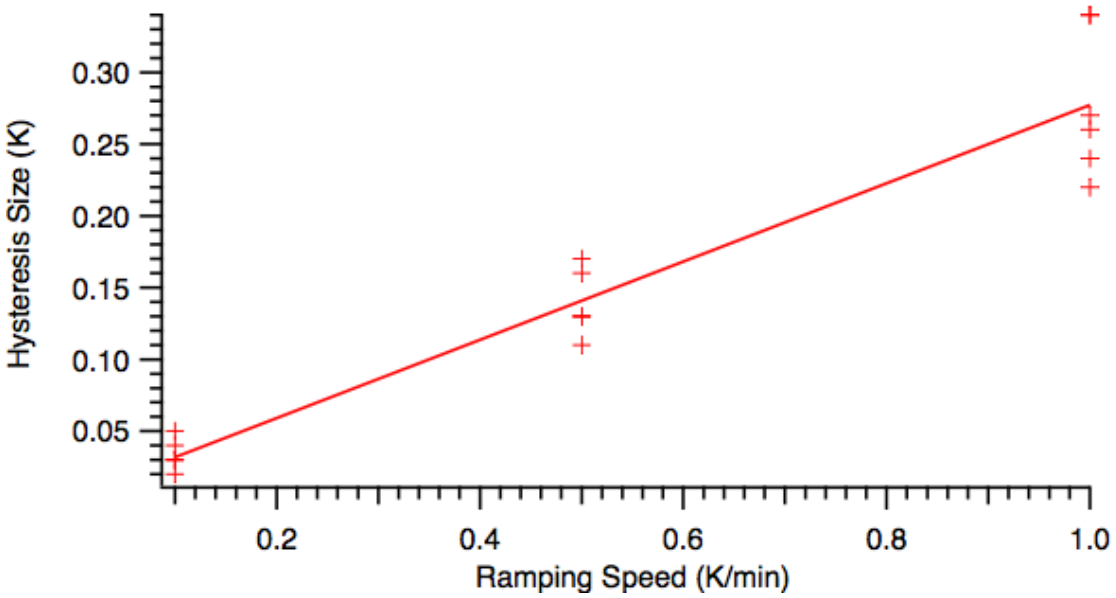

Figure 2.3: This is a graph of the width of the hysteresis curves plot against its ramping speed. This data was then fit to a linear model.

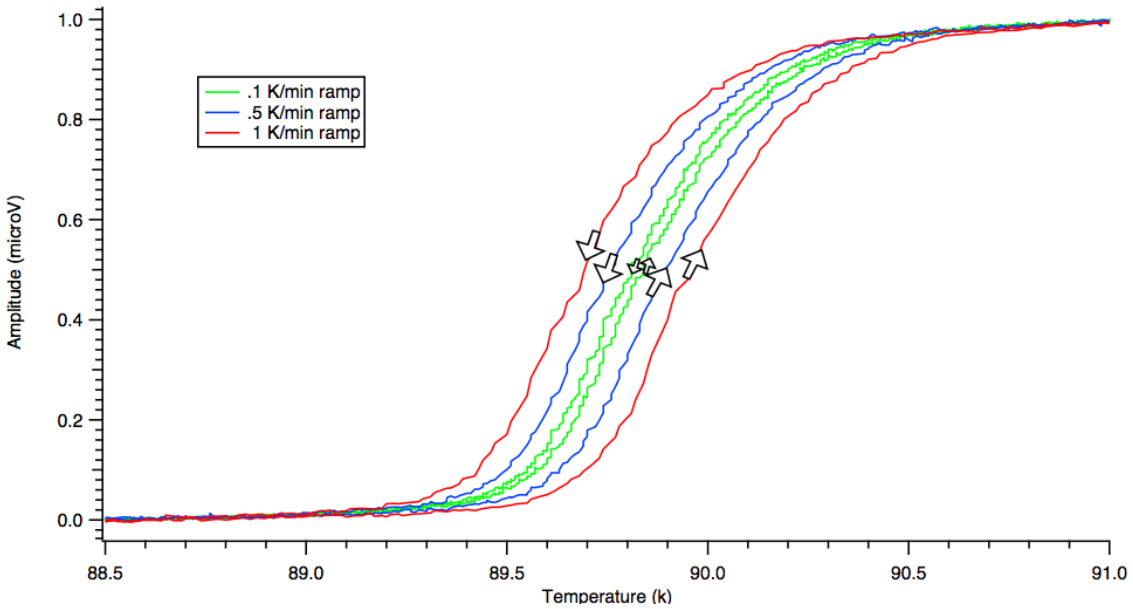

Figure 2.4: This is the data collected when ramping one sample at several different rates: 1K/min, 0.5K/min, and 0.1K/min. The arrows indicate the direction of the ramping.

The real value of T_c lies inside the hysteresis curves shown in Figure 2.4. This can be calculated by taking the average of the temperature values at the same voltage. For this experiment, all samples were ramped at 0.1 K/min in order to reduce the error seen from the hysteresis effect.

2.2 Raman Spectroscopy

Theory

Raman spectroscopy is a material measurement technique based off of the Raman effect. The Raman effect occurs when light waves interact with a crystalline lattice, and in turn the polarization of the lattice's electrons as well as the bonds between atoms. This effect comes about through inelastic light scattering. More specifically, a photon will interact with a lattice and cause it to be in a "virtual state" [Col12]. This virtual state is not a full absorption of the photon. Instead, it is a perturbation of the molecule which excites or de-excites vibrational or rotational energy states [Col12]. Therefore, it is considered an inelastic scattering process since a non-resonant photon is scattering the vibrational/rotational modes of the molecules

instead of absorbing its energy. If the molecule scatters with the same energy (elastic scattering), it is called Rayleigh scattering. If the energy of the incident photon gets stored/released as either vibration or rotations in the molecule then that energy difference will be seen in the output of the scattered light. This means that the scattered light has a shift in wavelength. If the scattered light has lower energy than the incident photons it is a Stokes Raman scattering. If the scattered light has higher energy than the incident photons it is a anti-Stokes Raman scattering (see Figure 2.5).

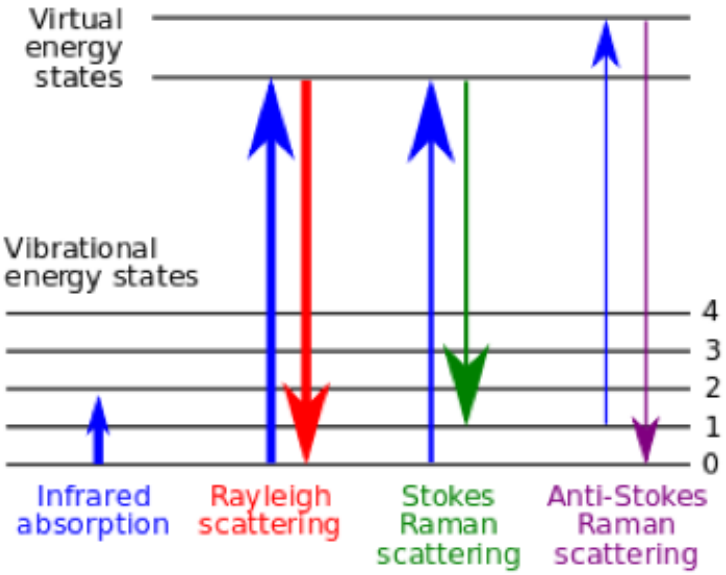

Figure 2.5: This depicts the transitional state excitation that occurs during Raman spectroscopy. There is one elastic scattering effect (Rayleigh) and two inelastic scattering effects (Stokes and Anti-Stokes).

This experimental technique is extremely useful in studying materials since it allows us to probe the lattice without damaging the sample. Raman spectroscopy can be used to characterize materials, measure temperature, find crystallographic orientation, among many other things [Dou08]. In this experiment, we use Raman Spectroscopy as a method of characterizing the phonon vibrational modes in the lattice. A given solid will have phonon modes that are characteristic of that specific lattice structure and the impurities in the sample. In addition, Raman spectroscopy can be used to observe other low frequency excitations of the solid, such as plasmons, magnons, and superconducting gap excitations [Dou08].

This is especially useful in studying the isotope effect since the oxygen-18 substitution into the lattice structure is not ideal and not consistent between different batches. Therefore, knowing the phonon modes of the oxygen-16 sample and that of the oxygen-18 sample we can verify what percentage of oxygen that was actually substituted [Hew+99]. This percentage is important in understanding the electronic properties of the material in ARPES as well as explaining the T_c shift from magnetometry.

It is conventional for Raman shifts to be measured in units of inverse length (cm^{-1}). This can easily can easily be converted to energy as needed. To convert between spectral wavelength and wavenumber shift in the Raman spectrum, the following is used:

$$\Delta w = \left(\frac{1}{\lambda_0} - \frac{1}{\lambda_1}\right) \tag{2.1}$$

where Δw is the Raman shift in wavenumber, λ_0 is the incoming excitation wavelength, and λ_1 is the outgoing Raman spectrum wavelength [Col12].

Experimental Setup

In a typical Raman experiment, a polarized laser beam (circularly polarized in our case) is focused onto a sample, and the scattered light is collected and dispersed by a high-resolution spectrometer to obtain the frequency spectrum. Since the Stokes/Anti-Stokes Raman effect occurs when the incident laser wavelength is not on resonance with the lattice vibrations, various filters must be used to reject all the light that is on resonance. This is especially important because the inelastic scattered Raman light is very weak compared to the elastic Rayleigh scattering (on the order of 10^7 times less powerful) [GLA]. Therefore the spectrometers must have good background light rejection and sensitive detectors.

In this experimental setup (Figure 2.6), the excitation source is a 532 nm Argon ion laser (at approximately 20 mW). A lens collects the scattered light and focuses it into the entrance slit of a triple spectrometer. This spectrometer consists of three

sections, each of which has a diffraction grating. In the first two sections stray light is rejected by the gratings. In the last section the light is dispersed by the final grating and gets detected by a charge-coupled device, CCD. The resolution achieved by this setup is about 1 cm^{-1}.

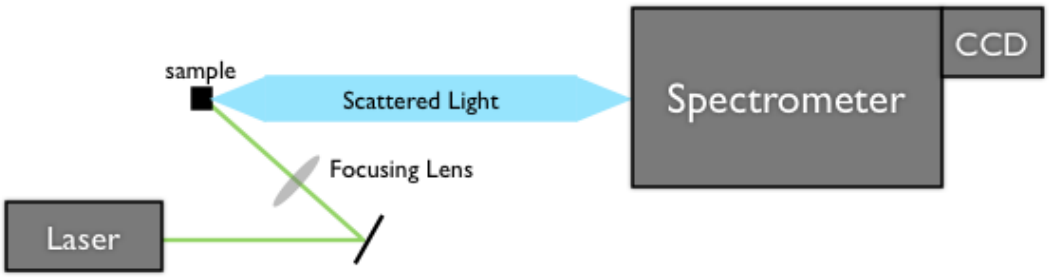

Figure 2.6: Block diagram of the Raman spectrometer setup.

2.3 Angle Resolved Photoemission Spectroscopy (ARPES)

Angle resolved photoemission spectroscopy is an experimental technique that studies electronic properties of solids, specifically the energy and momentum space of electrons in a lattice. Both energy and momentum are conserved in this system and this allows us to study the probability that a particle with a certain momentum has a specific energy. This probability is called the spectral function and it is related to the Heisenberg uncertainty principle [EV15]. The spectral function describes the distribution of an electron's uncertainty in a specific state of the band structure.

The basic theory behind ARPES is based on Einstein's photoelectric effect [Ein05]. The process of photoemision occurs when a photon interacts with the electrons in a material. The electrons absorb the energy of the incoming photon and get emitted from the material as a photoelectron. The energy of the photoelectron is therefore dependent on the energy of the incoming photon and the work function (the amount of energy needed for an electron to escape from its parent

atom) [Dou08].

More specifically:

$$E_{kinetic} = \hbar\omega - |E_i| - \Phi \tag{2.2}$$

Here $E_{kinetic}$ is the kinetic energy of the emitted photo-electrons, $\hbar\omega$ is the energy of the incoming photon, $|E_i|$ is the initial energy of the electron in the solid (the amount of energy needed to bring an electron to the Fermi level), and Φ is the work function of the solid. Properties of materials are mainly determined by the electrons that are close to the Fermi energy. So by studying the energy of these emitted photo-electrons, we can see the number of states per energy that can be occupied at each energy level (also known as the density of states) [Sim13].

By analyzing the angles of emission from the surface (defined in Figure 2.7) we can also get information about the momentum of electrons in the crystal. This relationship can be seen in Equation 2.3 [DHS03]:

$$\mathbf{p} = \sqrt{2mE_{kinetic}} * (sin\theta \cdot \hat{k}_x + cos\theta * sin\phi \cdot \hat{k}_y) \tag{2.3}$$

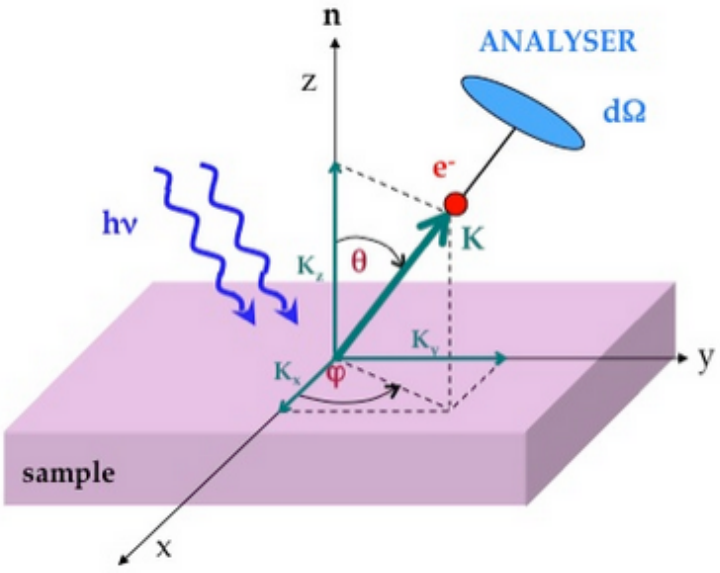

Figure 2.7: Photoelectron emission angles Φ and θ. [SN14]

The momentum resolution allows us to look at the anisotropic properties of

solids that are determined by the low energy electron band [Dou08]. The electron information that we get from measuring the emission angle (Figure 2.7) tells us the momentum of electrons that live in the x-y lattice plane. In other words, it is only the momentum information of electrons in the Cu-O planes which is useful since this is the layer that is responsible for superconductivity. This is one of the reasons why the method of ARPES is so useful in studying these materials. ARPES works best on studying 2D surfaces and we can treat BSCCO as a quasi-2D material (i.e. just the copper-oxide planes).

2.3.1 Synchrotron ARPES

Throughout the field, ARPES is most commonly performed at synchrotron facilities. These facilities produce light by accelerating high energy electrons around a ring. These electrons then go through a series of magnets with alternating pole directions called undulators. Since electrons have charge, the alternating north and south poles of the magnets cause the electrons to oscillate which produces light radiation. This light is the final synchrotron light used to study the materials.

There are several advantages to using synchrotron light beams. First off, they have a wide range of tunable photon energy. At some facilities this range can be as drastic as 9 eV light to 100 eV light [Dou08]. This is useful specifically when studying the antinode which requires photons with larger momenta to reach the edge of the Fermi surface (see Laser ARPES section). Another useful feature is the tunable polarization of the light. By changing the directions of the undulators we can get both linearly and circularly polarized light [Kim08].

2.3.2 Laser ARPES

Although synchrotron light is important to study HTS, there are several disadvantages to using these facilities. Trips to synchrotron facilities are time consuming and expensive. They also use high energy photons. Therefore, a complementary technique is to use laser light. The Dessau lab has a home-built ARPES setup that

uses low energy laser light instead of synchrotron beams. Using low energy lasers (7 eV) as a photon source has several important advantages over the traditional synchrotron technique.

Most importantly, lasers provide a higher flux of lower energy photons which gives better resolution in both momentum and energy (see Figure 2.8). Lasers also provide a cheaper alternative to synchrotron trips as well as an easier way to change properties of the incoming photons (i.e. polarizations) with just a few optics [Dou08]. Laser ARPES also allows better resolution over shorter time periods (more flux/count rate of electrons). This is important because materials degrade in ultra high vacuum (UHV). The faster the measurements can be taken, the less damage to each sample.

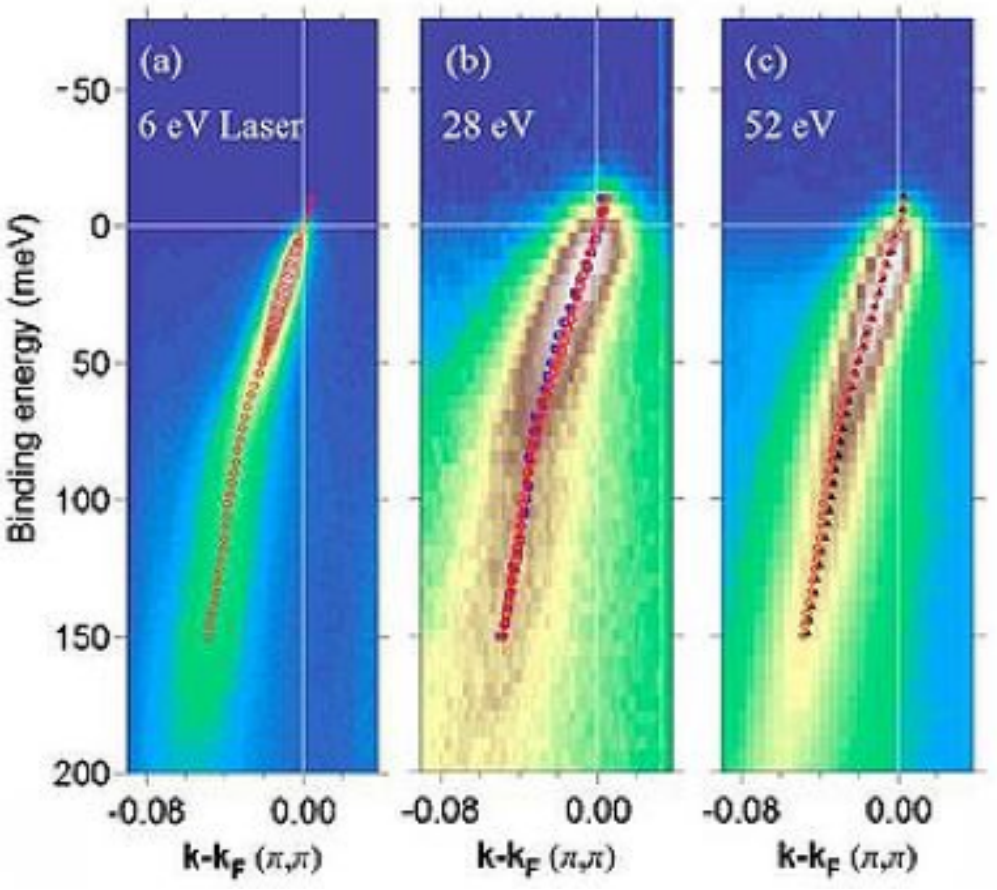

Figure 2.8: Experimental resolution of the spectral function using three different energy light sources. The improvement on resolution is visibly significant when a 6 eV laser is used to probe the system instead of 20-50 eV synchrotron light. [Kor+05]

Another advantage to using low energy laser ARPES is decreased surface sensi-

tivity. Looking at Figure 2.9 we see that at smaller energies (6eV) the mean free path of photons is larger than the mean free path at higher energies (20-50 eV). Therefore at lower energies, these photons travel farther into the sample and the photoelectrons emitted represent the properties of electrons from the bulk of the sample. All of this indicates that these measurements are less surface sensitive than synchrotron ARPES so the surface quality of the samples does not effect the spectra of electron states as much.

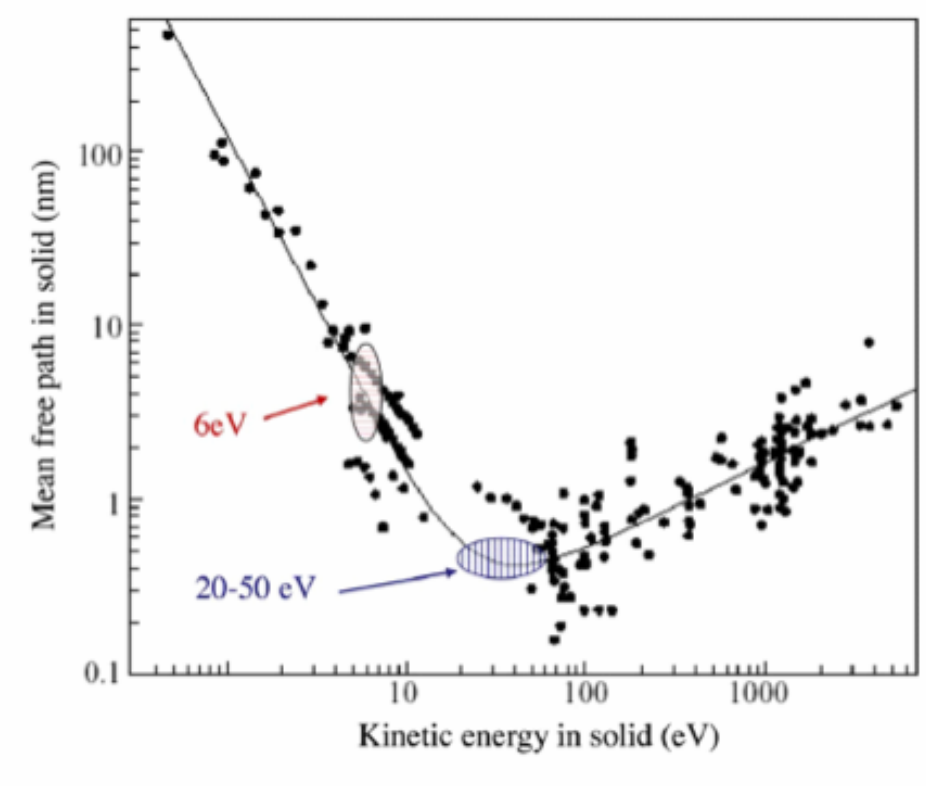

Figure 2.9: As kinetic energy of light in solid decreases, the mean free path in the solid increases. This is important because we can study electrons in the bulk of material so surface effects matter less. [SD79] [Dou08]

Although the momentum resolution is improved using laser ARPES, the amount of momentum space measured decreases (Figure 2.10). When there is less photon energy, we see less of the Fermi surface. The momentum space that we do see is better resolved but we see less of it than if we were to use high energy photons. This is a problem when studying the isotope effect because the 7 eV photons do not have enough energy to study the antinode portion of the Fermi surface. So we

can not compare the electron velocity, superconducting gap, and other properties along both the node and the antinode. In order to study the antinode, we need to use synchrotron energies but this reintroduces the poor resolution of high energy photons which prevent us from seeing isotope effect.

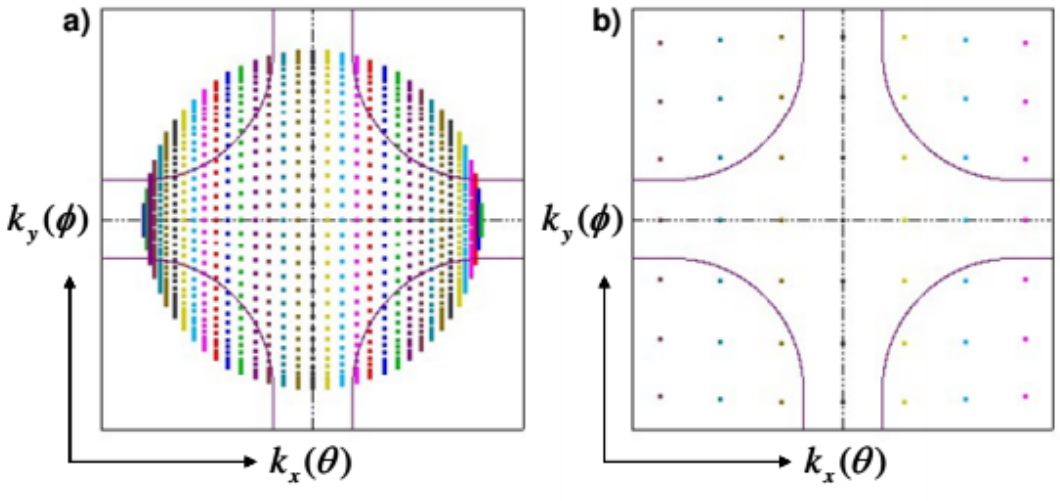

Figure 2.10: This is a visual of the trade-off between better momentum resolution and studying a larger momentum area. a) shows more momentum resolution but the area studied does not cover the full Fermi surface. b) shows less resolution but measurements are taken throughout the entire Fermi surface. [Dou08]

2.3.3 Experimental Setup

There are three main components to the laser ARPES setup.

Sample Manipulator

The sample manipulator has 5 axis manipulation - 3 translational and 2 rotational degrees of freedom. This allows for a more precise alignment of the sample lattice structure with respect to the incoming photons. This is important because alignment is very sensitive and the better we can align the crystal structure with the experimental setup the more accurately we can make cuts in the Fermi surface.

Sample Chamber

Once the sample is mounted on the sample manipulator, it is placed in the

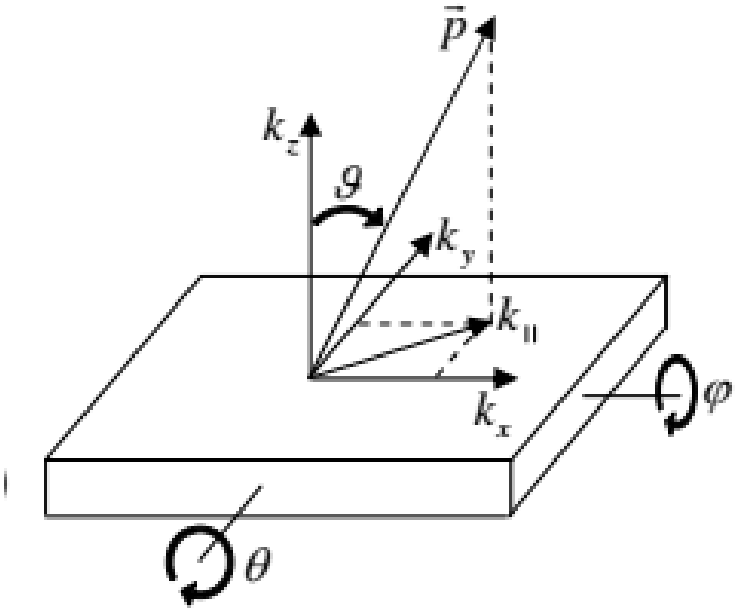

Figure 2.11: 5-axis manipulator which allows us to move in the x, y, z, ϕ, and θ directions. This helps us achieve better sample alignment. [Dou08]

sample chamber which is held at ultra-high vacuum (10^{-11} Torr). The sample is cleaved in situ to provide a clean surface. BSCCO will naturally cleave in between the Bi-O layers due to weaker Van der Waal forces in these layers [Dou08].

Electron Analyzer

Once the photo-electrons leave the sample, they travel with a certain momentum and energy to a hemispherical analyzer. This analyzer has a 30 degree momentum window with resolutions of 0.1 degree and 1 meV [Dou08]. The analyzer consists of two concentric hemispheres with a voltage difference between the hemispheres. By varying the voltage between the hemispheres a certain energy window of electrons is allowed to pass through to the other side of the hemisphere. If the electrons are not in this window of allowable energies they will collide with the outer wall (if they have too much energy) or with the inner wall (if they have too little energy). If an emitted photoelectron passes through the hemispheres it then hits a detector which magnifies the electron signal. The magnified signal then gets counted with a CCD. The output signal

gives us information on the angle and energy of the electron which can be be converted to a kinetic energy and momentum picture of the sample's spectral function.

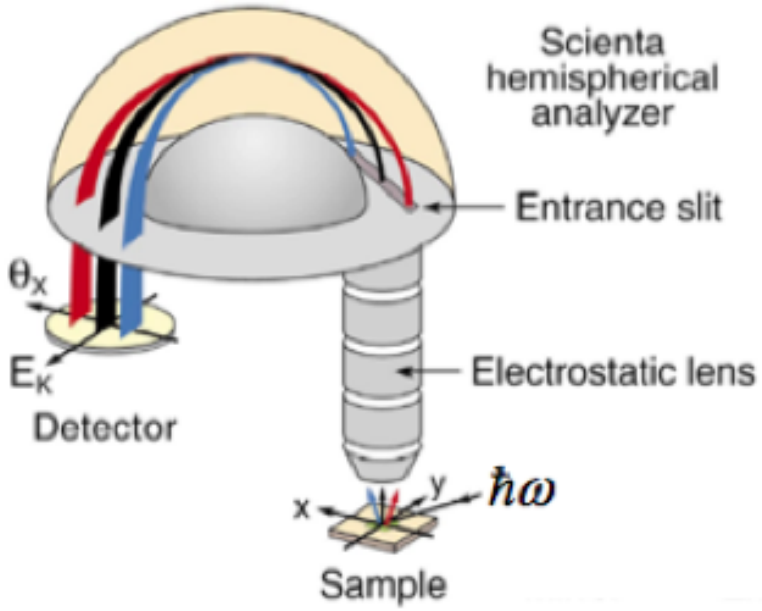

Figure 2.12: Hemispherical analyzer diagram showing how electrons of different energies pass through the analyzer onto a detector that outputs momentum and energy information [Dou08].

Chapter 3

Results

3.1 Magnetometry Data

Figure 3.1 shows magnetometry data measured for two different batches (batch 13 and batch 16) of isotope samples, each of which were grown/substituted independently. Since the growing/substitution process is not perfect, there will be discrepancies (of shift values) between batches of the same material. Each sample was measured multiple times and T_c was calculated at various points along the curve, specifically at 0.8, 0.5, 0.2 of the maximum amplitude. This data shows just how much T_c varies between batches and within each sample itself. Each T_c curve is not uniform across the transition width. This has to do with the fact that these samples are not perfect. They have many impurities which can cause small sub-regions of the sample to super-conduct at slightly different temperatures than other regions. This determines the transition width of the sample. In both of these batches we see that the T_c at half the amplitude have values that are closer to T_c measurements at the top of the transition showing that the transition is less defined at lower parts of the transitioning phase.

There is also a significant difference in the isotope shift between batches, with batch 16's shift being approximately 0.5 K larger than batch 13's shift. This indicates that the amount of oxygen substituted is not equal between batches of the same material. By analyzing this difference and comparing it to both Raman and

ARPES spectra, we will be able to develop a good characterization of the oxygen isotope effect.

Within these measurements, there is random error from the magnetometer. This uncertainty is approximately ±0.06 K for one standard deviation. Although this error has an effect on our measurements (especially since the expected isotope shift is only 0.5K) [Dou08], we can still make the claim that regardless of error, batch 16 has a larger shift than batch 13.

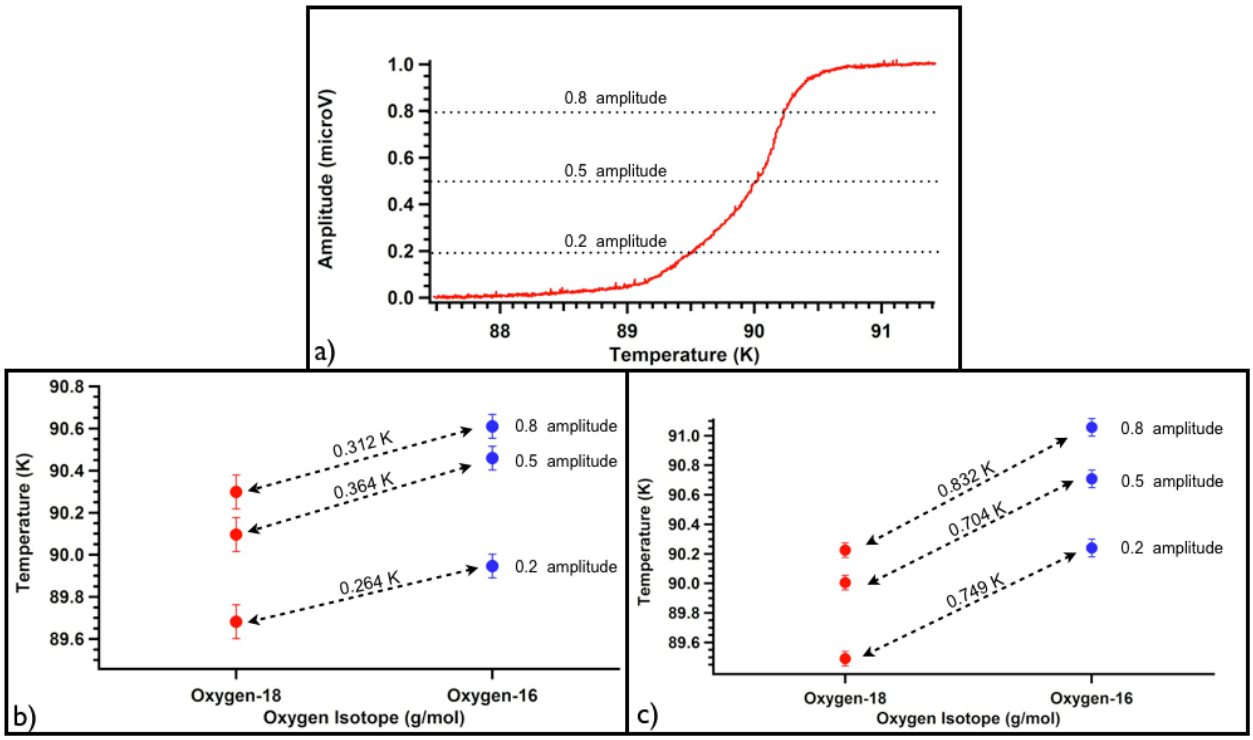

Figure 3.1: a) An example of normalized output data from the magnetometer. The macroscopic width and slope of the curve gives us insight to the microscopic properties in the material. Points at 0.8, 0.5, and 0.2 of the maximum amplitude were statistically analyzed and used to look at the isotope shift. b) The critical temperature isotope shift seen in batch 13 at 0.8, 0.5, and 0.2 of the maximum amplitude. c) The critical temperature isotope shift seen in batch 16 at 0.8, 0.5, and 0.2 of the maximum amplitude.

3.2 Raman Spectroscopy Data

The scattered energy that was added or taken away from the molecular vibrations due to Raman scattering occurs at a well defined frequency. Due to the fact that the molecule is interacting with its surroundings, however, each subset of molecules

will vibrate with a slightly different frequency. The result of this interaction is seen in the line shape of the Raman spectra. Instead of seeing a single perfectly defined peak, we see a broader peak encompassing a finite range of energies. The shape of the peaks gives us a lot of information on the molecular structure in the lattice. Each peak is a sum of all the individual vibrations and the exact frequency of these vibrations is dependent on its interactions with its neighbors [Bra07].

In each mode there are also two relaxation times that contribute to the linewidth. One is the time it takes for the vibrations to no longer be excited. The other is the time that it takes for the vibrational coherence of lattice movements to fade and in turn cause the vibrations to interfere with each other [Bra07]. In terms of this, the linewidth of Raman spectra can broaden if there is a large range of frequencies in the system.

Both of these aspects play a role in the isotope substitution experiment. Since not all the oxygen gets substituted, some oxygen-16 will still show up in Raman measurements. The summing of the two O16 and O18 frequencies produce a widening of the linewidth. Simultaneously, there will also be a shorter coherence lifetime since more than one frequency is involved. This also contributes to the shape of the linewidth.

Theoretically, from the simplest mass-spring model we expect an energy decrease of 3 meV, with the oxygen-18 material having a lower energy. Figure 3.2 shows the stokes Raman spectra of an oxygen-16 and oxygen-18 sample from two different batches. In batch 16, there is an energy decrease of 3.5 meV and a linewidth broadening of 0.08 meV. In batch 13, there is an energy decrease of 3.24 meV and a linewidth broadening of 0.58 meV.

3.3 ARPES Data

In ARPES spectra, there are several identifying features of the electronic properties that describe the HTS system. For nodal data, the identifying feature is a kink in the energy dispersion at approximately 70 meV binding energy. The energy

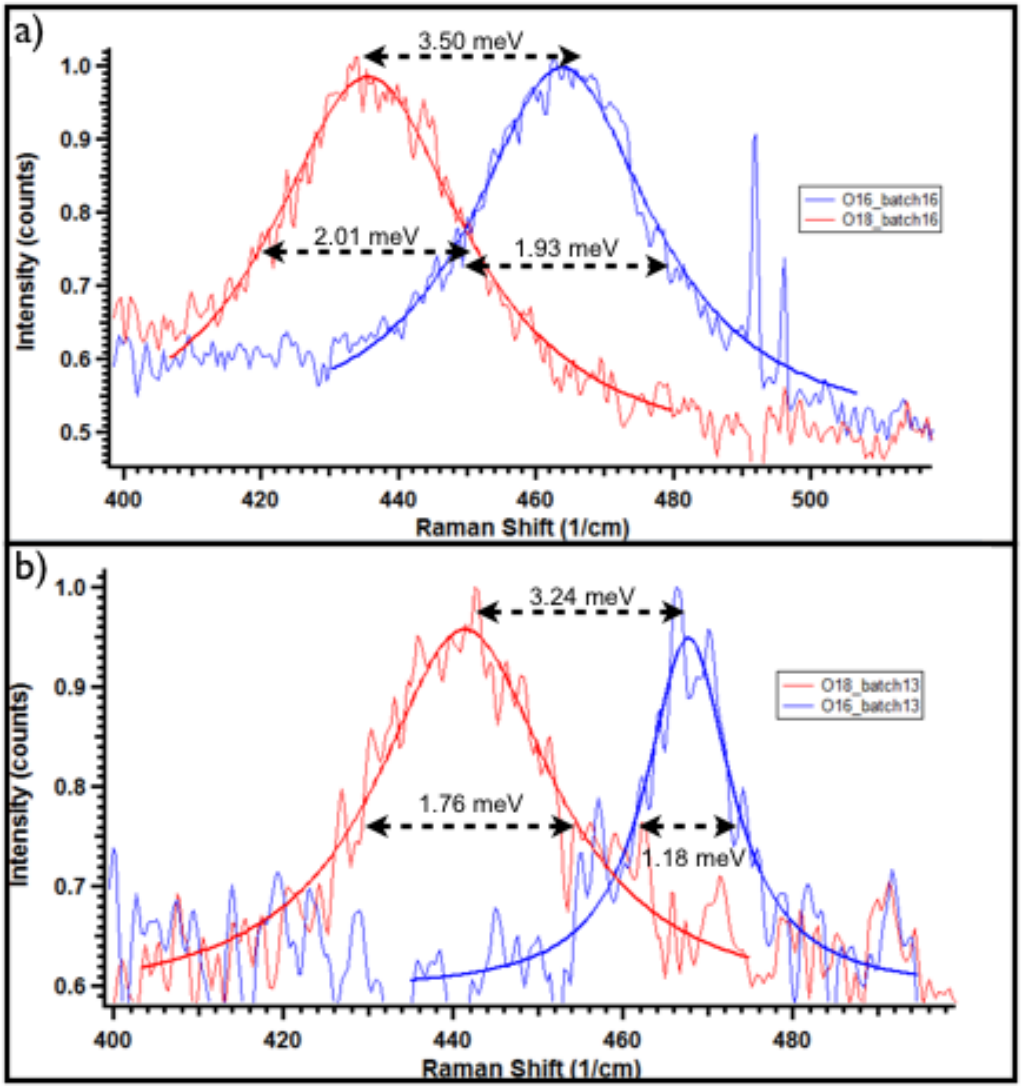

Figure 3.2: a) Raman spectroscopy data from batch 16 fit to a Lorentzian. b)Raman spectroscopy data from batch 13 fit to a Lorentzian.

kink represents the point at which the electrons are strongly interacting. Above this energy kink the dispersion band takes on a wider shape. This is due to the fact that electrons near the Fermi surface are strongly interacting quasiparticles that are "dressed" with more mass. Since these electrons have more mass, the energy dispersion widens. Therefore when a heavier mass is introduced in an isotope substitution, the frequency of the phonon vibration decreases (see Raman spectra) and manifests as a shift in the kink energy. In the oxygen-18 material, the kink is predicted to be 3 meV smaller than in the oxygen-16 material [Dou08]. This shift shows that electrons at smaller binding energies (i.e. near the Fermi surface) see the isotope shift and are in turn interacting with phonons.

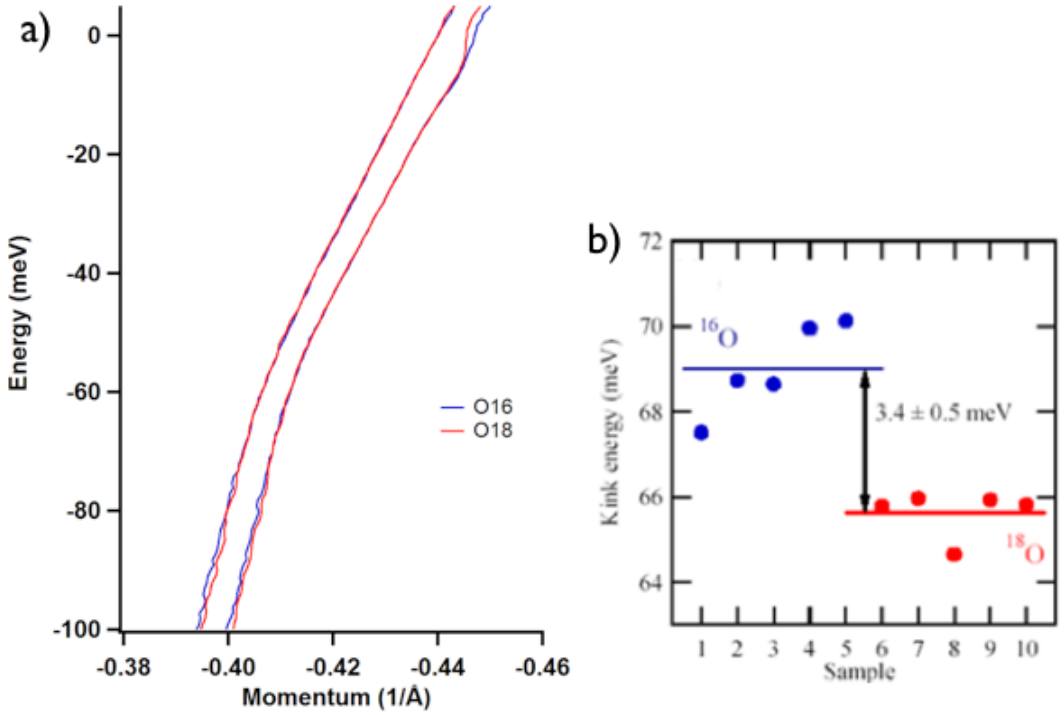

Figure 3.3: a) A fit of the lineshape of the 70 meV kink energy at two different cuts on the node for both O18 and O16 samples. These samples were taken from batch 13. No shift in kink energy is seen due to isotope substitution. Note, this data was collected and analyzed by Xiaoqing Zhou and Haoxiang Li. b)Previous experimental data showing a 3.4 meV kink shift due to isotope substitution [Dou08].

The ARPES data in Figure 3.3 measured isotope samples from batch 13 using 9eV synchrotron light and measured the 70 meV kink dispersion relation at two different cuts on the node. The resolution of this beamline setup was 5 meV and 0.15 degrees. In past experiments, the isotope shift at the 70 meV kink was measured to be approximately 3.4 meV [Dou08]. In this data though, we do not see a kink shift with the isotope substitution as shown in past experiments.

Figure 3.4 is a graph of the superconducting gap energy at different cuts along the node. This data shows the d-wave nature of the Fermi surface. As you move farther from the node the superconducting gap gets very large (almost 25 meV at 20 degrees from the node). For comparison, in conventional superconductivity the size of the gap was approximately 6 meV [Uch+03]. At the node (0 degrees in Figure 3.4), the gap goes to zero as expected.

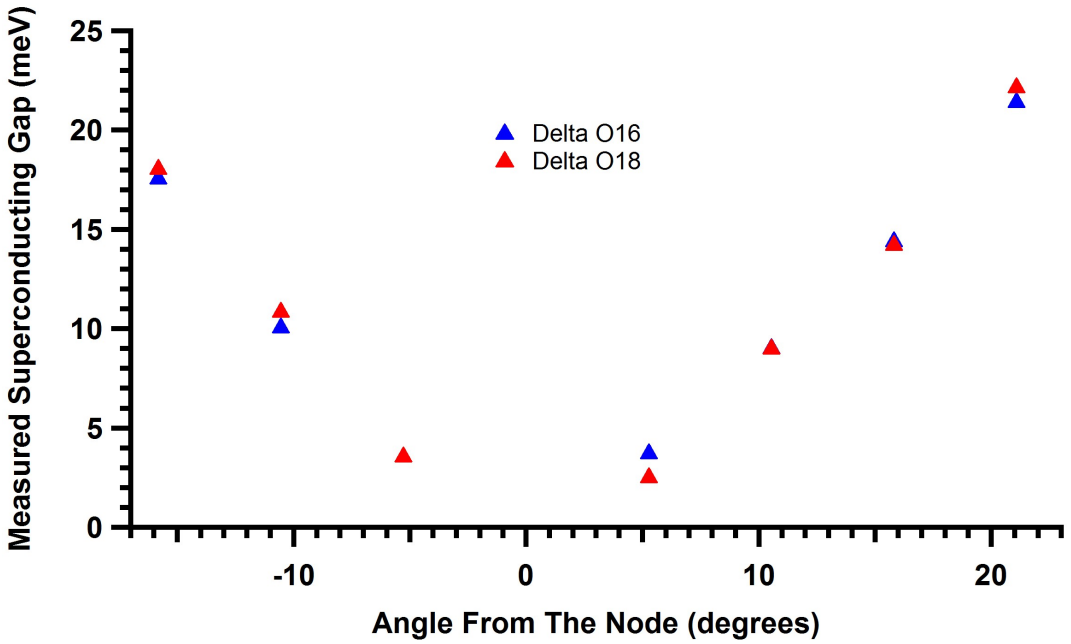

Figure 3.4: This is a measurement of the superconducting gap, Δ, at various angles from the node. The anisotropic gap size shows the d-wave symmetry of BSCCO Fermi surface. Note, this data was collected and analyzed by Xiaoqing Zhou and Haoxiang Li.

At the antinode, past experiments have shown that there is a 4 meV shift of the gap size with the Oxygen-16 isotope having a larger gap [Dou08]. This synchrotron data fails to reproduce that. In fact it is showing the opposite direction with the oxygen-18 slightly larger than the oxygen-16 gap. Also, the gap size itself seems to vary very little with isotope substitution as compared to the previous 4 meV shift seen.

Chapter 4

Conclusion

4.1 Discussion of Results

From the Raman spectroscopy and magnetometry data we are able to characterize the oxygen substitution in terms of a macroscopic superconductor phenomenon (T_c). We see that the direction and relative size of the O16 to O18 shift in the Raman data does not disagree with the magnetometry data. Batch 13 had a smaller T_c shift, smaller phonon frequency shift, and a larger phonon peak broadening than batch 16 indicating that batch 13 might have a smaller amount of oxygen-18 in its lattice structure. This is useful information because it reaffirms that our characterization techniques are complementing each other.

In the ARPES spectra (two batch 13 samples) no kink shift was seen. This result could be due to several factors: the physics of isotope shifts at the kink is not well understood, the samples were not well aligned, and there might be some sample to sample variation that is not being accounted for.

Although the experiments done in the past have shown a 3 meV isotope shift at the kink, these results have been difficult to reproduce in experiments since then. Therefore, the 3 meV expectation of these measurements may not be correct. On the other hand, if the lack of a shift is due to an experimental effect, such as sample alignment, replicating this data with the same samples should improve our analysis.

The gap size data has similar results as the kink shift and therefore can be

attributed to similar errors. The gap oxygen shift is very small and in the wrong direction (i.e. the O18 gap has slightly larger energy far from the node than the O16 gap) compared to expected results. This most likely points to an alignment or sample error.

4.2 Future Work

In the future there are many directions in which this experiment can go. Three of the most obvious are using laser ARPES on samples that were studied at the synchrotron (batch 13), studying the tomographic density of states, and measuring the doping dependence of the isotope shift.

Using laser ARPES we can remeasure batch 13 samples to see if we still see no kink shift. We can also study the temperature dependence of the electronic properties. This is called tomographic density of states. In other words, the gap size and the energy required to scatter the cooper pairs are measured across a continuum of temperatures ranging from well below to well above T_c. The temperature where the gap and scattering length meet should match the value of T_c measured from the magnetometer [Reb+13].

Finally, we can look at the doping dependence of these materials. Since the electronic properties HTS are highly dependent on the doping of the material, running a similar experiment on under-doped and over-doped BSCCO materials (as compared to the optimally doped samples in this experiment) will give us further insight in fully understanding the microscopic properties of these exotic materials.

Bibliography

[Ein05] Albert Einstein. "Über einen die Erzeugung und Verwandlung des Lichtes betreffenden heuristischen Gesichtspunkt". In: *Annalen der Physik* 322.6 (1905), pp. 132–148.

[Onn11] Heike Kamerlingh Onnes. "The disappearance of the resistivity of mercury". In: *Comm. Leiden* 122 (1911), p. 2.

[MO33] Walther Meissner and Robert Ochsenfeld. "Ein neuer effekt bei eintritt der supraleitfähigkeit". In: *Naturwissenschaften* 21.44 (1933), pp. 787–788.

[Frö50] H Fröhlich. "Theory of the superconducting state. I. The ground state at the absolute zero of temperature". In: *Physical Review* 79.5 (1950), pp. 845–856.

[Max50] Emanuel Maxwell. "Isotope effect in the superconductivity of mercury". In: *Physical Review* 78.4 (1950), p. 477.

[Rey+50] CA Reynolds et al. "Superconductivity of isotopes of mercury". In: *Physical Review* 78.4 (1950), p. 487.

[BCS57] John Bardeen, Leon N Cooper, and J Robert Schrieffer. "Microscopic theory of superconductivity". In: *Physical Review* 106.1 (1957), pp. 162–164.

[TS62] P Townsend and J Sutton. "Investigation by electron tunneling of the superconducting energy gaps in nb, ta, sn, and pb". In: *Physical Review* 128.2 (1962), p. 591.

[SD79] MP Seah and WA Dench. "Quantitative electron spectroscopy of surfaces: a standard data base for electron inelastic mean free paths in solids". In: *Surface and interface analysis* 1.1 (1979), pp. 2–11.

[BM86] J George Bednorz and K Alex Müller. "Possible highT c superconductivity in the Ba- La- Cu- O system". In: *Zeitschrift für Physik B Condensed Matter* 64.2 (1986), pp. 189–193.

[Bla92] Frank J Blatt. *Modern physics*. McGraw-Hill, 1992.

[Mye93] Kirsten Luther Myers. *The role of reduced dimensionality in the new perovskite superconductors*. Tech. rep. Stanford Univ., CA (United States), 1993.

[She+93] Z-X Shen et al. "Anomalously large gap anisotropy in the a-b plane of Bi 2 Sr 2 CaCu 2 O 8+ δ". In: *Physical review letters* 70.10 (1993), p. 1553.

[Roh94] James William Rohlf. "Modern Physics from aalpha to Z0". In: *Modern Physics from aalpha to Z0, by James William Rohlf, pp. 664. ISBN 0-471-57270-5. Wiley-VCH, March 1994.* 1 (1994).

[Zha+97] GM Zhao et al. "Evidence for polaronic supercarriers in the copper oxide superconductors". In: *Nature* 385.6613 (1997), pp. 236–238.

[CSB99] JP Carbotte, E Schachinger, and DN Basov. "Coupling strength of charge carriers to spin fluctuations in high-temperature superconductors". In: *Nature* 401.6751 (1999), pp. 354–356.

[Dai+99] Pengcheng Dai et al. "The magnetic excitation spectrum and thermodynamics of high-Tc superconductors". In: *Science* 284.5418 (1999), pp. 1344–1347.

[Hew+99] Kevin C Hewitt et al. "Isotope shift of the 5 9 0-cm-1 Raman feature in underdoped Bi 2 Sr 2 Ca Cu 2 O 8+ δ". In: *Physical Review B* 60.14 (1999), R9943.

[Sca99] DJ Scalapino. "The cuprate pairing mechanism". In: *Science* 284.5418 (1999), pp. 1282–1283.

[Sjö01] Mårten Sjöström. "Hysteresis modelling of high temperature superconductors". In: (2001).

[ZKC01] Guo-meng Zhao, H Keller, and K Conder. "Unconventional isotope effects in the high-temperature cuprate superconductors". In: *Journal of Physics: Condensed Matter* 13.29 (2001), R569.

[She+02] Z-X Shen et al. "Role of the electron-phonon interaction in the strongly correlated cuprate superconductors". In: *Philosophical magazine B* 82.13 (2002), pp. 1349–1368.

[DHS03] Andrea Damascelli, Zahid Hussain, and Zhi-Xun Shen. "Angle-resolved photoemission studies of the cuprate superconductors". In: *Rev. Mod. Phys.* 75 (2 2003), pp. 473–541. DOI: 10.1103/RevModPhys.75.473. URL: http://link.aps.org/doi/10.1103/RevModPhys.75.473.

[Hof03] Hoffman, Jennifer. "A Search for Alternative Electronic Order in the High Temperature Superconductor Bi2Sr2CaCu2O8+x by Scanning Tunneling Microscopy". PhD thesis. University of California, Berkeley, 2003.

[Uch+03] H Uchiyama et al. "Photoemission studies in MgB 2". In: *Physica C: Superconductivity* 385.1 (2003), pp. 85–90.

[Gwe+04] G-H Gweon et al. "An unusual isotope effect in a high-transition-temperature superconductor". In: *Nature* 430.6996 (2004), pp. 187–190.

[HTG04] J Hwang, T Timusk, and GD Gu. "High-transition-temperature superconductivity in the absence of the magnetic-resonance mode". In: *Nature* 427.6976 (2004), pp. 714–717.

[USG04] GS Uhrig, KP Schmidt, and M Grüninger. "Unifying magnons and triplons in stripe-ordered cuprate superconductors". In: *Physical review letters* 93.26 (2004), p. 267003.

[Kor+05] JD Koralek et al. "Laser ARPES, the sudden approximation, and quasiparticle-like peaks in Bi2Sr2CaCu2O8+ delta". In: *arXiv preprint cond-mat/0508404* (2005).

[Bra07] Michael Bradley. *Curve Fitting in Raman and IR Spectroscopy: Basic Theory of Line Shapes and Applications*. Tech. rep. Thermo Fisher Scientific, 2007.

[Che+07] Xiao-Jia Chen et al. "Phonon-mediated superconducting transitions in layered cuprate superconductors". In: *Physical Review B* 75.13 (2007), p. 134504.

[Mal07] Stuart RC Malin. "GAUSS, CARL FRIEDRICH (1777-1855)". In: *Encyclopedia of Geomagnetism and Paleomagnetism* (2007), p. 279.

[Dou08] Douglas, J Fraser. "The isotope effect on the electronic structure of high temperature superconductors". PhD thesis. University of Colorado, Boulder, 2008.

[Kim08] Kwang-Je Kim. "Characteristics of synchrotron radiation". In: *Physics of Particle Accelerators*. Vol. 184. 1. AIP Publishing. 2008, pp. 565–632.

[Ami11] Eran Amit. "Investigating the Mechanism of High Temperature Superconductivity by Oxygen Isotope Substitution". PhD thesis. Technion-Israel Institute of Technology, Department of Physics, 2011.

[Col12] Norman Colthup. *Introduction to infrared and Raman spectroscopy*. Elsevier, 2012.

[GK12] Sachin Gupta and Umanath Kamath. *Make accurate temperature measurements using semiconductor junctions*. 2012. URL: `http://www.eetimes.com/document.asp?doc_id=1279718` (visited on 03/10/2015).

[Reb+13] TJ Reber et al. "Prepairing and the "filling" gap in the cuprates from the tomographic density of states". In: *Physical Review B* 87.6 (2013), p. 060506.

[Sim13] Steven H Simon. *The Oxford solid state basics*. Oxford University Press, 2013.

[SN14] Arlette Sohanfo Ngankeu. "Low-energy electronic structure and Fermi surface topology of the itinerant metamagnet SrRuO". PhD thesis. 2014.

[EV15] Thomas Eversberg and Klaus Vollmann. *Spectroscopic Instrumentation*. Springer, 2015.

[GLA] BILRC Laser lab GLA. *Raman Spectroscopy*. California Institute of Technology.